ELSEVIER

Materials Science and Engineering B 134 (2006) 54–58

MATERIALS SCIENCE & ENGINEERING B

www.elsevier.com/locate/mseb

ZnO nanopowders fabricated by dc thermal plasma synthesis

T.S. Ko [a,1], S. Yang [a], H.C. Hsu [a], C.P. Chu [a], H.F. Lin [b], S.C. Liao [b], T.C. Lu [a,*], H.C. Kuo [a], W.F. Hsieh [a], S.C. Wang [a]

[a] *Department of Photonics & Institute of Electro-Optical Engineering, National Chiao Tung University,1001 Tahsueh Road, Hsinchu 30050, Taiwan*
[b] *Materials Research Laboratories, Industrial Technology Research Institute, 195 Section 4 Chung Hsing Road, Chutung, Hsinchu 310, Taiwan*

Received 14 April 2006; received in revised form 2 June 2006; accepted 17 July 2006

Abstract

Ultrafine ZnO nanopowders were successfully synthesized by the dc thermal plasma process with a high production rate of 1.2 kg/h. The combination of plasma was found to affect the nanoparticles morphology. Both X-ray diffraction and Raman spectrum analysis confirmed a high quality wurtzite structure of the ZnO nanopowders. Photoluminescence study exhibited strong ultraviolet emission corresponding to the near band edge emission in the ZnO nanopowders. Random laser action observed in the ZnO nanostructures by optical pumping demonstrated high optical and crystal quality of the ZnO nanopowders fabricated by the dc thermal plasma synthesis.

Keywords: dc thermal plasma; ZnO nanopowders; Exciton

1. Introduction

ZnO nanostructures are very promising because of the wide band gap (3.37 eV) and large free exciton binding energy (60 meV) which exhibit a wide range of applications including field emission displays, nano-photonic devices, piezoelectric transducers, varistors, phosphors, and transparent conducting films [1–3]. To date various techniques have been used to synthesize ZnO nanoparticles including chemical or physical methods [4]. The former are thermal hydrolysis technique [5], hydrothermal processing [6], and sol–gel method [7–9]. The latter are spray pyrolysis [10], vapor condensation method [11] and thermochemical decomposition of metal organic precursors [12]. Nevertheless, the main problems of most methods have been the poor throughput efficiency and the difficulty in size control.

In this paper, we report a rapid fabrication technique of ZnO nanopowders by dc thermal plasma synthesis with a high production rate. By changing gas combination and the gas flow rate, different morphology and varied growth rate of the ZnO nanopowders can be achieved. In this study, the spherical and rod-like nanopowders were obtained by dc thermal plasma synthesis and were investigated by using X-ray diffraction (XRD), scanning electron microscopy (SEM), and Raman spectra and demonstrated high crystal quality. Furthermore, pulsed pumping PL result revealed the random laser action in rod-like ZnO nanopowders indicating that high crystal quality of the nanopowders could be efficiently fabricated by dc plasma synthesis.

2. Experiments

In this study, ZnO nanopowders were synthesized in a novel dc plasma reactor operated at 70 kW and atmospheric pressure as shown in Fig. 1. Commercial zinc powders (Alfa Aesar) containing impurities of Cr, Fe and Pb less than 50 ppm were used as the raw materials. The Zn powders were fed into plasma flame through N_2 carrier gas and subsequently underwent vaporization, oxidation and quench processes. The ZnO nanopowders synthesis rate could be 1.2 kg/h. Sample A was synthesized by using N_2 and Ar as plasma gases with the flow ratio of 1:1 and sample B was synthesized by using only N_2. Flow rates of the plasma, carrier and quenching gases were 15, 10 and 3000 slm, respectively. The specific surface area of the as-grown ZnO nanopowders was determined by a nitrogen gas adsorption instrument (Micrometrics ASAP 2010). Nitrogen elemental analysis was done with a nitrogen/oxygen determination (LECO Corporation, TC-436). The chemical composition

* Corresponding author. Tel.: +886 3 5131234; fax: +886 3 5716631.
E-mail addresses: tsko.eo93@nctu.edu.tw (T.S. Ko), timtclu@faculty.nctu.edu.tw (T.C. Lu).
[1] Tel.: +886 3 5712121x52962; fax: +886 3 5716631.

0921-5107/$ – see front matter © 2006 Elsevier B.V. All rights reserved.
doi:10.1016/j.mseb.2006.07.019

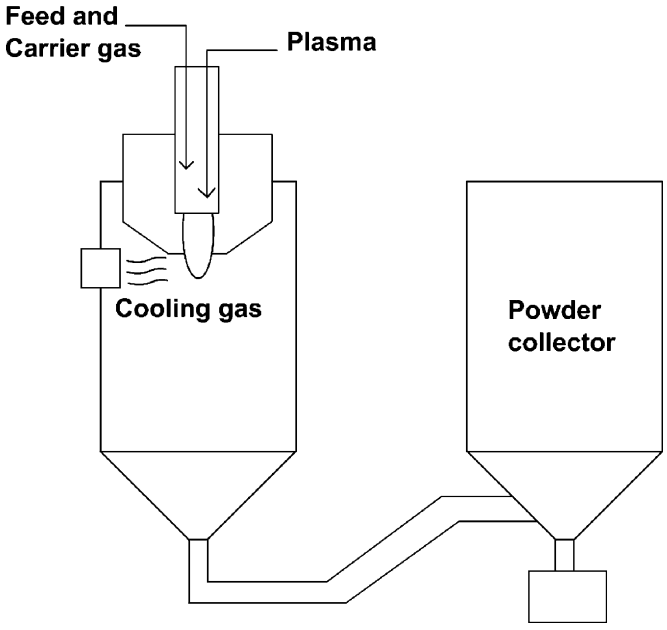

Fig. 1. Schematic of the dc plasma reactor.

of the nanoparticles was analyzed by an inductively coupled plasma-mass spectrometer (ICP-MS, Spectro-P). The characteristics of the resulting nanopowders are listed in Table 1. The morphology of the samples was observed by SEM. Different shapes of two samples can be observed, i.e. rod-like and spherical ZnO nanopowders for samples A and B, respectively. The phase identity and crystallite size of the ZnO nanopowders were examined by using an X-ray diffractometer (XRD, Philip PW1700) and Raman spectra. The X-ray diffractometer was operated at 40 keV and 40 mA with a Cu Kα radiation. The scanning step size and the collection time for each step were set at 0.02° and 5 s, respectively. An Ar ion laser emitting a 488 nm wavelength and 150 mW output power was used as the excitation source of the laser Raman scattering spectrometer. The scattered light was collected in the backscattering geometry. The CW-photoluminescence measurement was performed by using a 20 mW He–Cd laser with an emission wavelength of 325 nm. The collected light was dispersed by a TRIAX-320 spectrometer and was detected by a photomultiplier tube. The frequency-tripled output ($\lambda = 355$ nm) of a mode-locked Nd:YAG laser, with 1 kHz repetition rate and 500 ps pulse width was used as optical pumping source for the room temperature optical pumping experiment. The excitation laser beam was focused onto the sample surface at normal incidence and the light emission was collected at 45° to the surface.

Table 1
Characteristics and composition of the ZnO nanopowders grown by dc thermal plasma

Sample	Shape	Surface area ($m^2\,g^{-1}$)	Plasma-forming gas	Carrier gas	N (ppm)
A	Rod-like	7.5	50% Ar, 50% N_2	N_2	1200
B	Sphere	15.1	100% N_2	N_2	1770

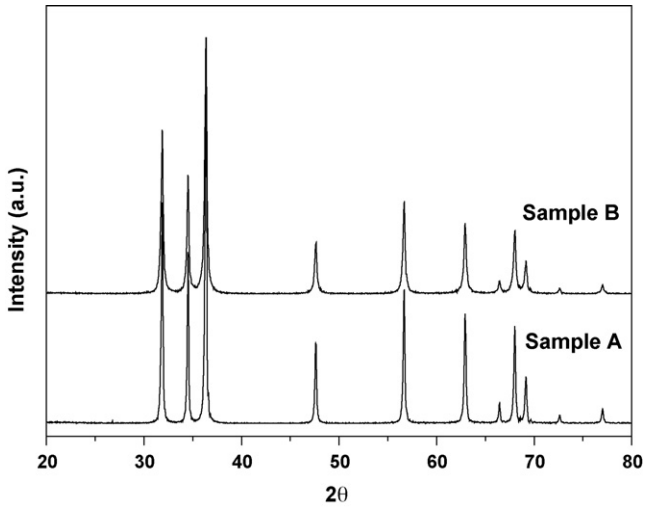

Fig. 2. XRD results of ZnO nanopowders.

3. Results and discussion

The XRD patterns of the rod-like and spherical ZnO nanopowders for samples A and B are shown in Fig. 2, where two samples show similar diffraction peak positions. No peaks were observed as phases of ZnO precursors and impurities, indicating high purity of the ZnO nanopowders obtained by dc thermal plasma synthesis. All diffraction peaks could be identified as a hexagonal ZnO phase with lattice constant of $a = 3.25$ Å and $c = 5.12$ Å. The strong intensities relative to the background signal also indicated high crystallization quality of the ZnO nanopowders. The FWHM of the XRD is often used to estimate the grain sizes of the powders from the Scherrer formula [13]

$$D = \frac{0.9\lambda}{\beta \cos\theta} \quad (1)$$

where λ is the X-ray wavelength, θ is the Bragg's angle and β is the pure full width of the diffraction line at half of the maximum intensity. After calculation from the XRD results, the average size along [1 0 1] direction of samples A and B were 30 and 31 nm. On the other hand, the β value of all peaks in XRD results also revealed quality and crystallization of both shapes ZnO nanopowders. Clearly, sample A has smaller β value than sample B indicating the higher quality and crystallization of sample A than sample B.

The SEM images of these two synthesized ZnO nanopowders are shown in Fig. 3. Rod-like morphology of sample A showed an average diameter of 30 nm and an average length of 100–200 nm. Spherical morphology of sample B showed an average grain size of 30 nm. The specific surface areas of the nanopowders listed on Table 1 varied from 7.2 to 15.1 m^2/g, indicating a certain extent of agglomeration in both kinds of the nanopowders. The different types of plasma gases could affect the nanopowders morphology and fewer N_2 plasma condition should favor formation of rod-like nanopowders. In this technique, dc plasma supplied the necessary energy of synthesis process. The precursors, zinc powders, with an average particle

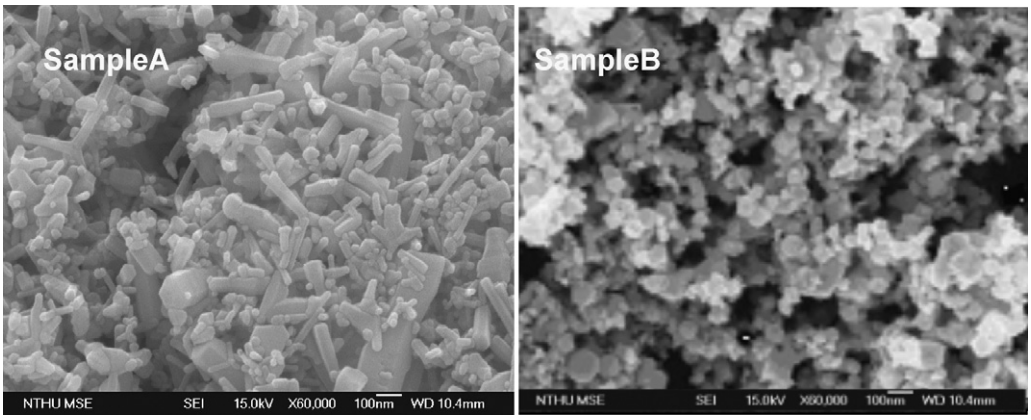

Fig. 3. Representative SEM images showing morphologies of ZnO nanostructures: sample A (rod-like) and sample B (sphere).

size of 10 μm were injected into plasma by carrier gas and subsequently further caused reaction within 10^{-2}–10^{-1} s. Therefore, this method is suitable for high production rate of industry.

Typical Raman spectra of the ZnO nanopowders are shown in Fig. 4. ZnO with hexagonal wurtzite structure belongs to the C_{6v} space group. According to group theory, there are eight $\mathbf{q} = 0$ phonon modes exist, where $\mathbf{q}$ is the wave vector, i.e., two E2, one A1-(TO), one A1-(LO), one E1(TO), one E1(LO), and two B1 modes. The A1 and E1 modes are both Raman and infrared active, the two B1 modes are silent, and the E2 modes are Raman active. Therefore, the most intense peak at 436.7 cm^{-1} was the well-known E2 symmetry mode for hexagonal ZnO. The peaks at 379.5, 529.3 and 578.7 cm^{-1} agreed with phonon vibration frequencies of A1-(TO), A1-(LO) and E1-(LO) modes of the hexagonal ZnO, respectively. The weak, broad peak around 410 cm^{-1} was E1-(LO) [14]. The feature peak at 332 cm^{-1} was a second-order structure of ZnO, interpreted as $2E_2$(M) [15]. The Raman result also demonstrated that the samples were composed of hexagonal ZnO. According to results done by Rajalakshmi et al. [16], the peak of E1(LO) mode of Raman spectra depend on the size of ZnO nanoparticles. However, there were no obvious differences between sample A and sample B in our study. Since

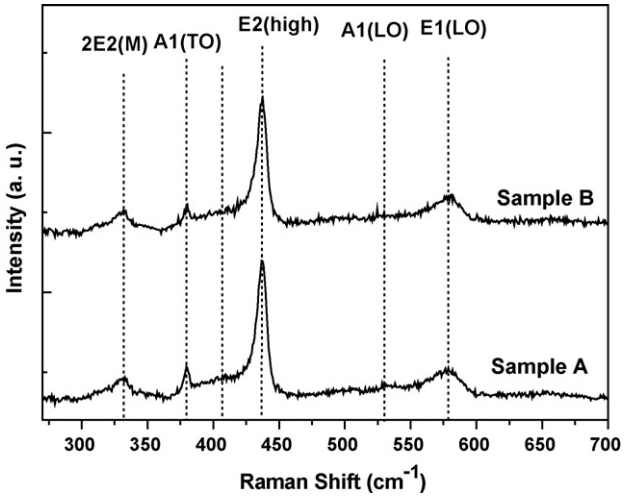

Fig. 4. Raman spectra of both shapes ZnO nanopowders.

dimensions of both kinds ZnO nanopowders in our experiment were bigger than the Bohr diameter, phonon confinement effect could not be observed.

PL spectra of the synthesized samples measured at room temperature are shown in Fig. 5. Both samples showed strong and sharp ultraviolet emissions at about 390 nm, which was attributed to the near band edge emission of the wide-bandgap ZnO [17]. The slight red-shift of the emission peak compared to the typical emission of ZnO bandgap might be due to the effect of the thermal accumulation caused by laser heating [18]. Sample B showed a weak broad defect-related emission at 510 nm (2.43 eV) while sample A showed a relatively strong green emission peak. The green emission was attributed to the recombination of electrons in singly occupied oxygen vacancies with photogenerated holes in the valence band. Comparing to the similar results reported previously [19,20]. The vacancy defect centers exist primarily in the thin (∼30 nm) electron-depletion layer near the surface of the ZnO. The intensity emitted from sample A was obviously stronger than sample B. The UV emission/green emission ratio decreased with decreasing the size of ZnO nanopowders since the reduction of surface area. Except for the slight differences of morphology and size between two samples caused different sampling area, moreover, heating, scattering and thus poor light collection in sample B and the higher crystallization quality of sample A might be the reason of it's higher PL intensity.

Fig. 6 shows the optical pumping PL spectra for samples A and B. Fig. 5(a) shows the emission spectrum measured at different location on sample A. The laser action was observed with several narrow and sharp peaks and the threshold pumping intensity was obtained to be about 35 MW/cm^2. The spectral position of each mode changed with the excitation locations and the mode spacing was irregular. In addition, the lasing mode could be observed at different detection angle. The lasing thresholds observed in the nanopowders varied by orders of magnitude, most likely due to the degree of the powder aggregation. Cao et al. reported that multiple scatterings with photon amplification resulted in random laser action in highly disordered ZnO polycrystalline films and powders. There were many closed loop paths for light formed by optical scattering. Laser oscillations would occur in those closed loops where loss was less than opti-

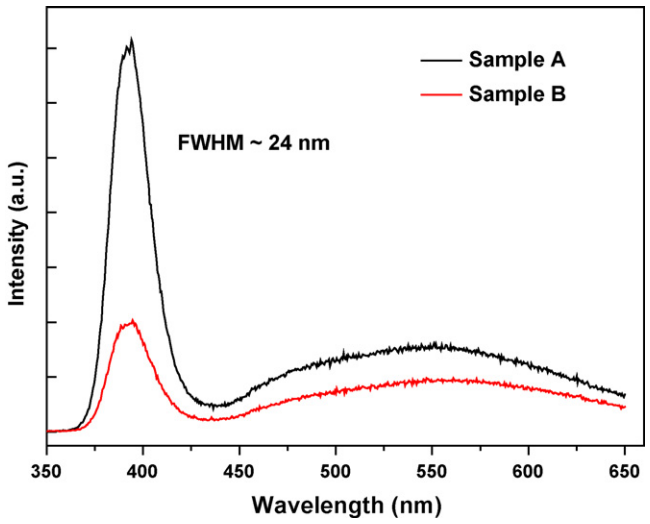

Fig. 5. Room temperature PL spectra of both shapes ZnO nanopowders.

cal amplification. The lasing modes in the emission spectra were from different loops formed by scattering in the nanopowders of sample A. In Fig. 5(a), the emission peaks of lasing modes are about 388 nm and the PL peak wavelength is 395 nm under the high excitation. The energy difference between these peaks was calculated to be about 56 meV, which was close to the exciton binding energy. This energy difference suggested that the PL emission might be contributed by the free exciton emission. However, there might be no enough density of energy state for excitons to overcome the optical loss. Instead, the band-to-band emission occurred due to plenty carriers accumulated and obtained enough gain in the ZnO nanostructures for stimulated emission. On the other hand, as shown in Fig. 5(b) for sample B, only a broad spontaneous emission peak at the same pumping intensity as used in sample A was observed. Wu et al. demonstrated that the lasing threshold increased as the ZnO nanopowder size decreased [21]. This could be one of the possible reasons because the optical loss might be larger than the amplification gain in the sample B with a smaller ZnO nanopowder size. In addition, the crystal quality of sample B revealed by XRD and PL measurement could account for the high lasing threshold in comparison with the sample A.

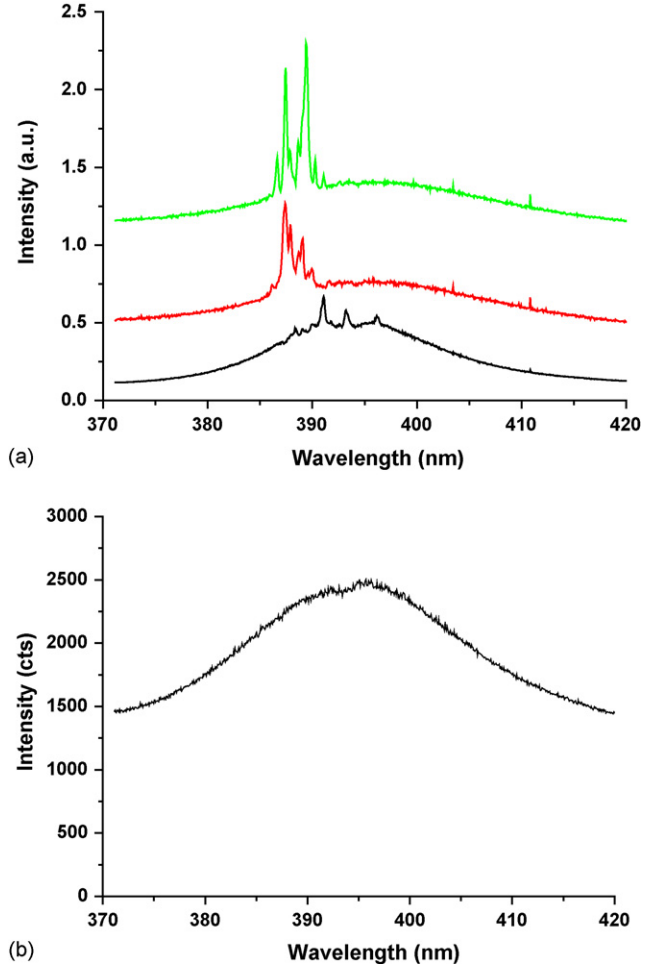

Fig. 6. Optical pumping spectra of ZnO nanopowders for (a) sample A at different location area with the same pumping intensity and (b) sample B.

4. Conclusion

In conclusion, ZnO nanopowders were successfully fabricated by a novel dc thermal plasma synthesis process with a high production rate. The growth rate and shapes of the ZnO nanopowders could be controlled by changing plasma gas combination and flow rate. The measurement results of X-ray diffraction, scanning electron microscopy and Raman spectroscopy showed that the samples were composed of wurtzite phase ZnO. The photoluminescence exhibited a strong ultraviolet peak corresponding to the near band edge emission and a weak broad green peak arising from the defect-related emission. Moreover, random laser actions observed only in rod-like ZnO nanopowders were probably due to the coherent feedback scattering in the structure, and indicated high crystal quality of the ZnO nanopowders. This production technique of the ZnO nanopowders could be applied to several practical applications such as UV absorption, NO_X decomposition, deodorization, antibacterial treatment and the target in molecule beam epitaxy system [22,23].

Acknowledgement

This work was partly supported by NSC of the Republic of China under Contract No. NSC 93-2112-M009-035.

References

[1] S.H. Jo, J.Y. Lao, R.A. Farrer, T. Baldacchini, J.T. Fourkas, Appl. Phys. Lett. 83 (2003) 4821.
[2] D.C. Reynolds, D.C. Look, B. Jogai, C.W. Litton, T.C. Collins, W. Harsch, G. Cantwell, Phys. Rev. B 57 (1998) 12151.
[3] B.M. Ataev, A.M. Bagamadova, V.V. Mamedov, A.K. Omaev, Mater. Sci. Eng. B 65 (1999) 159.
[4] K.J. Klabunde, Nanoscale Materials in Chemistry, John Wiley and Sons, New York, 2001, pp. 88.
[5] H.K. Park, D.K. Kim, C.H. Kim, J. Am. Ceram. Soc. 80 (1997) 743.
[6] S.I. Hirano, Ceram. Bull. 66 (1987) 1342.
[7] D. Vorkapic, T. Matsoukas, J. Am. Ceram. Soc. 81 (1998) 2815.
[8] V.R. Palkar, Nanostruct. Mater. 11 (1999) 369.

[9] Y.X. Li, K.J. Klabunde, Chem. Mater. 4 (1992) 611.
[10] T.T. Kodas, Adv. Mater. 6 (1989) 180.
[11] C.G. Granqvist, R.A. Burhman, J. Appl. Phys. 47 (1976) 2200.
[12] G. Skanadan, Y.J. Chen, N. Glumac, B.H. Kear, Nanostruct. Mater. 11 (1999) 149.
[13] B.D. Cullity, Elements of X-ray of Diffractions, Addition-Wesley, Reading, MA, 1978, pp. 102.
[14] J. Ye, S. Gu, S. Zhu, T. Chen, W. Liu, F. Qin, L. Hu, R. Zhang, Y. Shi, Y. Zheng, J. Vac. Sci. Technol. A 21 (2003) 979.
[15] Y.C. Kong, D.P. Yu, B. Zhang, W. Fang, S.Q. Feng, Appl. Phys. Lett. 78 (2001) 407.
[16] M. Rajalakshmi, A. Arora, B.S. Bendre, S. Mahamuni, J. Appl. Phys. 87 (2000) 2445.
[17] K. Vanhusden, C.H. Seager, W.L. Warren, D.R. Tallant, J.A. Voigt, Appl. Phys. Lett. 68 (1995) 403.
[18] H. Cao, Y.G. Zhao, H.C. Ong, S.T. Ho, J.Y. Dai, J.Y. Wu, R.P.G. Zhao, Appl. Phys. Lett. 73 (1998) 3656.
[19] X.H.H. Wu, A. Yamilov, H. Noh, H. Cao, E.W. Seelig, R.P.H. Chang, J. Opt. Soc. Am. B 21 (2004) 159, 21.
[20] J.M. Calleja, M. Cardona, Phys. Rev. B 16 (1977) 3753.
[21] P. Zu, Z.K. Tang, G.K.L. Wong, M. Kawasaki, A. Ohtomo, H. Koinuma, Y. Segawa, Solid State Commun. 103 (1997) 459.
[22] M.D. Driessen, T.M. Miller, V.H. Grassian, J. Mol. Catal. A 131 (1998) 149.
[23] J. Villasenor, P. Reyes, G. Pecchi, J. Chem. Technol. Biotechnol. 72 (1998) 105.